

Prediction Error Meta Classification in Semantic Segmentation: Detection via Aggregated Dispersion Measures of Softmax Probabilities

Matthias Rottmann¹, Pascal Colling¹, Thomas Paul Hack²,
Robin Chan¹, Fabian Hüger³, Peter Schlicht³ and Hanno Gottschalk¹

¹University of Wuppertal, School of Mathematics and Natural Sciences

²University Leipzig, Faculty of Physics

³Volkswagen Group Innovation, COI Automation, Architecture and AI-Technologies

{rottman,pascal.colling,robin.chan,hanno.gottschalk}@uni-wuppertal.de

thomas-paul.hack@itp.uni-leipzig.de

{peter.schlicht,fabian.hueger}@volkswagen.de

Abstract

We present a method that “meta” classifies whether segments predicted by a semantic segmentation neural network intersect with the ground truth. For this purpose, we employ measures of dispersion for predicted pixel-wise class probability distributions, like classification entropy, that yield heat maps of the input scene’s size. We aggregate these dispersion measures segment-wise and derive metrics that are well-correlated with the segment-wise IoU of prediction and ground truth. This procedure yields an almost plug and play post-processing tool to rate the prediction quality of semantic segmentation networks on segment level. This is especially relevant for monitoring neural networks in on-line applications like automated driving or medical imaging where reliability is of utmost importance. In our tests, we use publicly available state-of-the-art networks trained on the Cityscapes dataset and the BraTS2017 data set and analyze the predictive power of different metrics as well as different sets of metrics. To this end, we compute logistic LASSO regression fits for the task of classifying $\text{IoU} = 0$ vs. $\text{IoU} > 0$ per segment and obtain AUROC values of up to 91.55%. We complement these tests with linear regression fits to predict the segment-wise IoU and obtain prediction standard deviations of down to 0.130 as well as R^2 values of up to 84.15%. We show that these results clearly outperform standard approaches.

1. Introduction

In recent years, deep learning has outperformed other classes of predictive models in many applications. In

some of these, *e.g.* autonomous driving or diagnostics in medicine, the reliability of a prediction is of highest interest. In classification tasks, the thresholding on the highest softmax probability or thresholding on the entropy of the classification distributions (softmax output) are commonly used approaches to detect false predictions of neural networks, see *e.g.* [9, 15]. Metrics like classification entropy or the highest softmax probability are usually combined with model uncertainty (Monte-Carlo (MC) dropout inference) and sometimes input uncertainty, cf. [8] and [15], respectively. These approaches have proven to be practically efficient for detecting uncertainty. Such methods have also been transferred to semantic segmentation tasks. See also [19] for further uncertainty metrics. The work presented in [13] makes use of MC dropout to model the uncertainty of segmentation networks and also shows performance improvements in terms of segmentation accuracy. This approach was applied in other works to model the uncertainty and filter out predictions with low reliability, cf. *e.g.* [12, 24]. In [10] this line of research was further developed to detect spacial and temporal uncertainty in the semantic segmentation of videos.

In this work we establish an approach for efficiently meta-classifying whether an inferred segment (representing a predicted object) of a semantic segmentation intersects with the ground truth or not, as similarly proposed for classification problems in [9]. The term *meta classification* has been used in the context of classical machine learning for learning the weights for each member of a committee of classifiers [16]. In terms of deep learning we use it as a shorthand to distinguish between a network’s own classification and the classification whether a prediction is “true” or “false”. In contrast to the work cited above, we aim at judg-

ing the statistical reliability of each segment inferred by the neural network. To this end, dispersion measures, like entropy, are applied to the softmax probabilities (the networks output) on pixel level yielding dispersion heat maps. We aggregate these heat maps over predicted segments alongside with other quantities derived from the network’s prediction like the segment’s size and predicted class. From this, we construct per-segment metrics. A commonly used performance measure for the quality of a segmentation is the intersection over union (*IoU* a.k.a. Jaccard index [11]) of prediction and ground truth. We use the constructed metrics as inputs to logistic regression models for meta classifying, whether an inferred segment’s *IoU* vanishes or not, i.e., predicting $IoU = 0$ or $IoU > 0$. Also, we use linear regression models for predicting a segment’s *IoU* directly, thus obtaining statements about the reliability of the network’s prediction. Our method only uses the softmax output of a semantic segmentation network and the corresponding ground truth. It can be equipped with any heat map obtained from pixel-wise uncertainty measures. Thus, any work on uncertainty quantification for semantic segmentation that yields new improved dispersion heat maps can be seamlessly integrated and leverages our method. Hence, we also provide a framework to evaluate the quality of pixel-wise uncertainty measures for semantic segmentation.

In our tests we use two publicly available datasets: Cityscapes [5] for the semantic segmentation of street scenes and BraTS2017 [2, 17] for brain tumor segmentation. For each of the two datasets we employ two state-of-the-art networks. We perform tests on validation sets and demonstrate that our segment-wise metrics are well correlated with the *IoU*; thus they are suitable for detecting false positives on segment level. For logistic regression fits we obtain values of up to 91.55% for the area under curve corresponding to the receiver operator characteristic curve (AUROC, see [7]). Predicting the segment-wise *IoU* via linear regression we obtain prediction standard deviations of down to 0.130 and R^2 values of up to 84.15%.

2. Pixel-wise dispersion metrics and aggregation over segments

A segmentation network with a softmax output layer can be seen as a statistical model that provides for each pixel z of the image a probability distribution $f_z(y|x, w)$ on the q class labels $y \in \mathcal{C} = \{y_1, \dots, y_q\}$, given the weights w and the data x . The predicted class in z is then given by

$$\hat{y}_z(x, w) = \arg \max_{y \in \mathcal{C}} f_z(y|x, w). \quad (1)$$

Dispersion or concentration measures quantify the degree of randomness in $f_z(y|x, w)$. Here, we consider two of those measures: *entropy* E_z (also known as *Shannon information* [22]) and *difference in probability* D_z , i.e. the

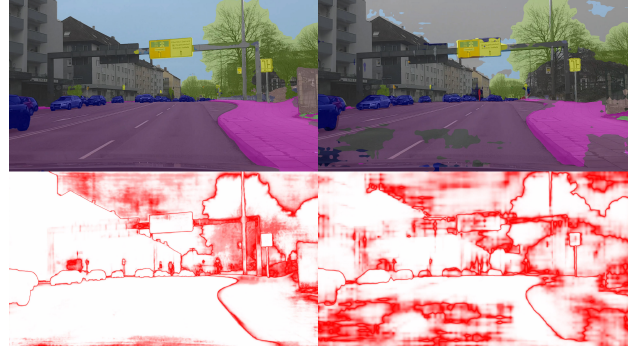


Figure 1. Segmentation example (top line) and heat map D_z (bottom line) for Xception65 (left column) and MobilenetV2 (right column). Original image is not part of the Cityscapes data set.

difference between the two largest softmax values:

$$E_z(x, w) = -\frac{1}{\log(q)} \sum_{y \in \mathcal{C}} f_z(y|x, w) \log f_z(y|x, w), \quad (2)$$

$$D_z(x, w) = 1 - f_z(\hat{y}_z(x, w)|x, w) + \max_{y \in \mathcal{C} \setminus \{\hat{y}_z(x, w)\}} f_z(y|x, w). \quad (3)$$

For better comparison, both quantities have been written as dispersion measures and been normalized to the interval $[0, 1]$: One has $E_z = D_z = 1$ for the equiprobability distribution $f_z(y|x, w) = \frac{1}{q}$, $y \in \mathcal{C}$, and $E_z = D_z = 0$ on the deterministic probability distribution ($f_z(y|x, w) = 1$ for one class and 0 otherwise). For the discussion of further dispersion measures, cf. [6]. The most direct method of uncertainty quantification on an image is the heat mapping of a dispersion measure as in figure 1.

For a given image x we denote by $\hat{\mathcal{K}}_x$ the set of connected components (segments) in the predicted segmentation $\hat{\mathcal{S}}_x = \{\hat{y}_z(x, w)|z \in x\}$ (omitting the dependence on the weights w). Analogously we denote by \mathcal{K}_x the set of connected components in the ground truth \mathcal{S}_x . For each $k \in \hat{\mathcal{K}}_x$, we define the following quantities:

- the interior $k_{in} \subset k$ where a pixel z is an element of k_{in} if all eight neighbouring pixels are an element of k
- the boundary $k_{bd} = k \setminus k_{in}$
- the intersection over union *IoU*: let $\mathcal{K}_x|_k$ be the set of all $k' \in \mathcal{K}_x$ that have non-trivial intersection with k and whose class label equals the predicted class for k , then

$$IoU(k) = \frac{|k \cap K'|}{|k \cup K'|}, \quad K' = \bigcup_{k' \in \mathcal{K}_x|_k} k'$$

- adjusted intersection over union IoU_{adj} : let $Q = \{q \in \hat{\mathcal{K}}_x : q \cap K' \neq \emptyset\}$, for reasons explained in section 5

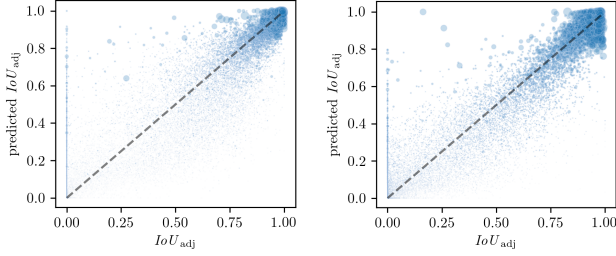


Figure 2. IoU_{adj} vs. predicted IoU_{adj} for all connected components predicted by Xception65 (left) and MobilenetV2 (right). Dot sizes are proportional to S .

	XC	MN		XC	MN
\bar{E}	-0.70139	-0.70162	\bar{D}	-0.85211	-0.84858
\bar{E}_{bd}	-0.44065	-0.41845	\bar{D}_{bd}	-0.60308	-0.52163
\bar{E}_{in}	-0.71623	-0.69884	\bar{D}_{in}	-0.85458	-0.82171
\tilde{E}	0.31219	0.36261	\tilde{D}	0.22797	0.30245
\tilde{E}_{in}	0.39195	0.42806	\tilde{D}_{in}	0.29279	0.35131
S	0.30442	0.47978	\tilde{S}	0.50758	0.71071
S_{bd}	0.44625	0.62713	\tilde{S}_{in}	0.50758	0.71071
S_{in}	0.30201	0.47708			

Table 1. Correlation coefficients ρ with respect to IoU_{adj} . Results are computed on the Cityscapes validation set, XC: DeepLabv3+Xception65 and MN: DeepLabv3+MobilenetV2.

we use in our tests

$$IoU_{adj}(k) = \frac{|k \cap K'|}{|k \cup (K' \setminus Q)|}$$

- the pixel sizes $S = |k|$, $S_{in} = |k_{in}|$, $S_{bd} = |k_{bd}|$
- the mean entropies \bar{E} , \bar{E}_{in} , \bar{E}_{bd} defined as

$$\bar{E}_{\#}(k) = \frac{1}{S_{\#}} \sum_{z \in k_{\#}} E_z(x), \quad \# \in \{-, in, bd\}$$

- the mean distances \bar{D} , \bar{D}_{in} , \bar{D}_{bd} defined in analogy to the mean entropies
- the relative sizes $\tilde{S} = S/S_{bd}$, $\tilde{S}_{in} = S_{in}/S_{bd}$
- the relative mean entropies $\tilde{\bar{E}} = \bar{E}\tilde{S}$, $\tilde{\bar{E}}_{in} = \bar{E}_{in}\tilde{S}_{in}$, and relative mean distances $\tilde{\bar{D}} = \bar{D}\tilde{S}$, $\tilde{\bar{D}}_{in} = \bar{D}_{in}\tilde{S}_{in}$

Typically, E_z and D_z are large for $z \in k_{bd}$. This motivates the separate treatment of interior and boundary measures. With the exception of IoU and IoU_{adj} , all scalar quantities defined above can be computed without the knowledge of the ground truth. Our aim is to analyze to which extent they are able to predict IoU_{adj} .

3. Numerical Experiments: Street Scenes

We investigate the properties of the metrics defined in the previous section for the example of a semantic segmentation of street scenes. To this end, we consider the

DeepLabv3+ network [3] for which we use a reference implementation in Tensorflow [1] as well as weights pretrained on the Cityscapes dataset [5] and available on GitHub. The DeepLabv3+ implementation and weights are available for two network backbones: Xception65, which is a modified version of Xception [4] and is a powerful structure intended for server-side deployment, and MobilenetV2 [21], a fast structure designed for mobile devices. Each of these implementations have parameters tuning the segmentation accuracy. We choose the following best (for Xception65) and worst (for MobilenetV2) parameters in order to perform our analysis on two very distinct networks. Note, that the parameter set for the Xception65 setting also includes the evaluation of the input on multiple scales (averaging the results) which increases the accuracy and also leverages classification uncertainty. We refer to [3] for a detailed explanation of the chosen parameters.

- DeepLabv3+Xception65: output stride 8, decoder output stride 4, evaluation on input scales 0.75, 1.00, 1.25 – $mIoU = 79.72\%$ on the Cityscapes validation set
- DeepLabv3+MobilenetV2: output stride 16, evaluation on input scale 1.00 – $mIoU = 61.85\%$ on the Cityscapes validation set

Example segmentations and heat maps of the two networks are displayed in figure 1. For both networks, we consider the output probabilities and predictions on the Cityscapes validation set, which consists of 500 street scene images at a resolution of 2048×1024 . We compute the 15 constructed metrics as well as IoU_{adj} for each segment in the segmentations of the images. In order to investigate the predictive power of the metrics, we first compute the Pearson correlation $\rho \in [-1, 1]$ between each feature and IoU_{adj} . We report the results of this analysis in table 1 and provide scatter plots of all features relative to IoU_{adj} in figure 4. Note, that in all computations, we only consider connected components with non-empty interior.

For both networks IoU_{adj} shows strong correlation with the mean distances \bar{D} and \bar{D}_{in} as well as with the mean entropies \bar{E} and \bar{E}_{in} . On the other hand, the relative counterparts are less correlated with IoU_{adj} . The relative segment size \tilde{S} for the DeepLabv3+MobilenetV2 network shows a clear correlation whereas this is not the case for the more powerful DeepLabv3+Xception65 network.

In order to find more indicative measures, we now investigate the predictive power of the metrics when they are combined. For the Xception65 net, we obtain 45,194 segments with non-empty interior of which 11,331 have $IoU_{adj} = 0$. For the weaker MobilenetV2 this ratio is 42,261/17,671. We would first like to detect segments with $IoU_{adj} = 0$, i.e., learn the meta classification task of identifying false positive segments based on our 15 metrics and the segment-wise averaged probability distribution

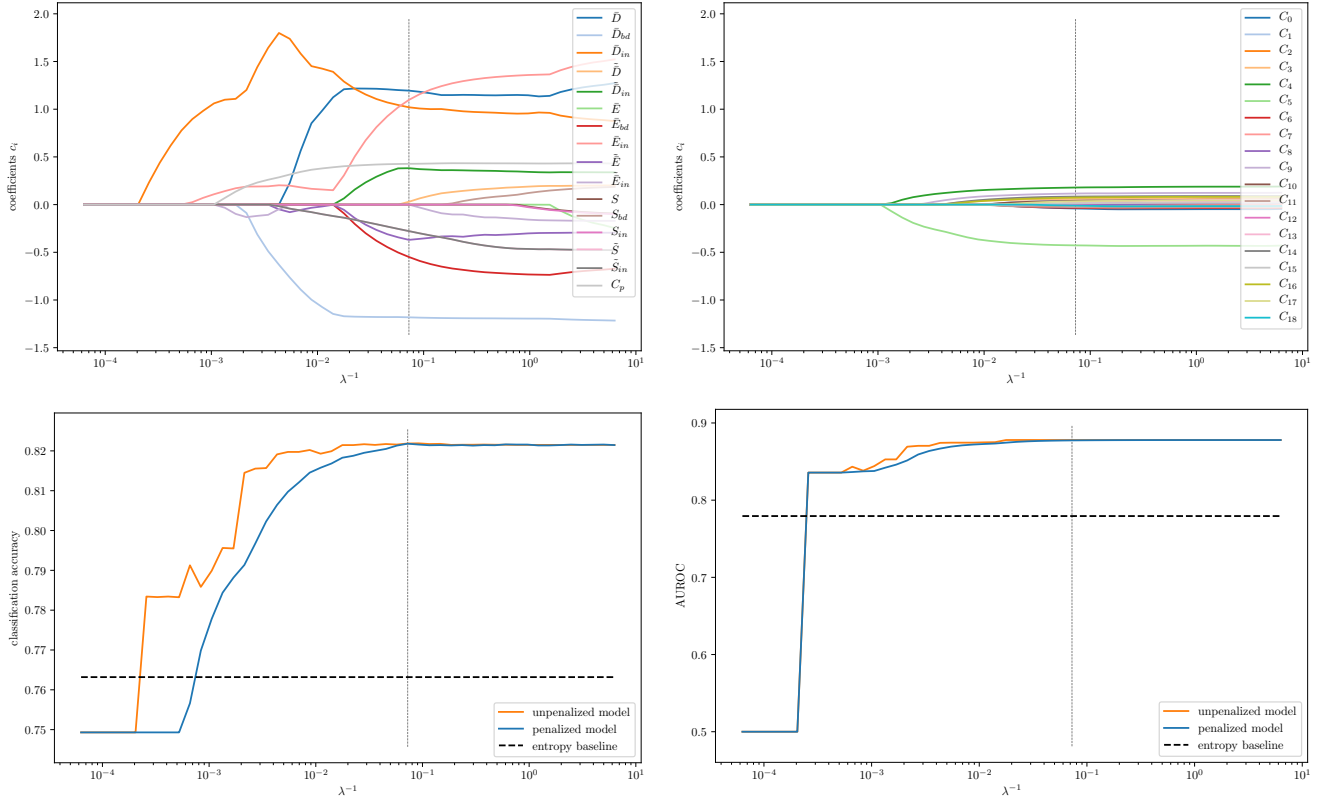


Figure 3. Results for the meta classification task $IoU_{\text{adj}} = 0, > 0$ for predictions obtained from the Xception65 net. (Top left): the weights coefficients for the 15 metrics computed with LASSO fits as function of λ^{-1} , C_p denotes the maximum of the absolute values of all weight coefficients for predicted classes. (Top right): like top left but showing coefficients for the 18 predicted classes. (Bottom left): meta classification rates for $IoU_{\text{adj}} = 0, > 0$. The blue line are the LASSO fits for different λ values, the orange line shows the performance of regular logistic regression fits ($\lambda = 0$) where the input metrics are only those that have non-zero coefficients in the LASSO fit for the current λ . (Bottom right) same as bottom left, but for AUROC. The vertical dashed lines indicate the λ value for which we obtained the best validation accuracy.

vectors. We term these (standardized) inputs x_k for a segment k . Further, let $y_k = \text{ceil}(IoU_{\text{adj}}) = \{0 \text{ if } IoU_{\text{adj}} = 0, 1 \text{ if } IoU_{\text{adj}} > 0\}$. The least absolute shrinkage and selection operator (LASSO, [23]) is a popular tool for investigating the predictive power of different combinations of input variables. We compute a series of LASSO fits, i.e., ℓ_1 -penalized logistic regression fits

$$\min_w \sum_i [-y_i \log(\tau(w^T x_i)) - (1 - y_i)(1 - \log(\tau(w^T x_i))) + \lambda \|w\|_1], \quad (4)$$

for different regularization parameters λ and standardized inputs (zero mean and unit standard deviation). Here, $\tau(\cdot)$ is the logistic function. Results for the Xception65 net are shown in figure 3.

The top left and top right panels show, in which order the weight coefficients w for each metric/predicted class become active. At the same time the bottom left and bottom right panels show, which weight coefficient causes which

amount of increase in predictive performance in terms of meta-classification rate and AUROC, respectively. The AUROC is obtained by varying the decision threshold of the logistic regression output for deciding whether $IoU = 0$ or $IoU > 0$.

The first non-zero coefficient activates the \bar{D}_{in} metric, which elevates the predictive power above our reference benchmark of choice, the mean entropy per component \bar{E} . Another significant gain is achieved when \bar{D}_{bd} and the predicted classes come into play. We obtain a meta-classification validation accuracy of up to 81.91% ($\pm 0.13\%$) and an AUROC of up to 87.71% ($\pm 0.15\%$) for Xception65. And also for the weaker MobilenetV2 we obtain 78.93% ($\pm 0.17\%$) classification accuracy and 86.77% ($\pm 0.17\%$) AUROC. We randomly choose 10 50/50 training/validation data splits and average the results, the numbers in brackets denote standard deviations of the averages. Additionally, the bottom line of figure 3 shows that there is almost no performance loss

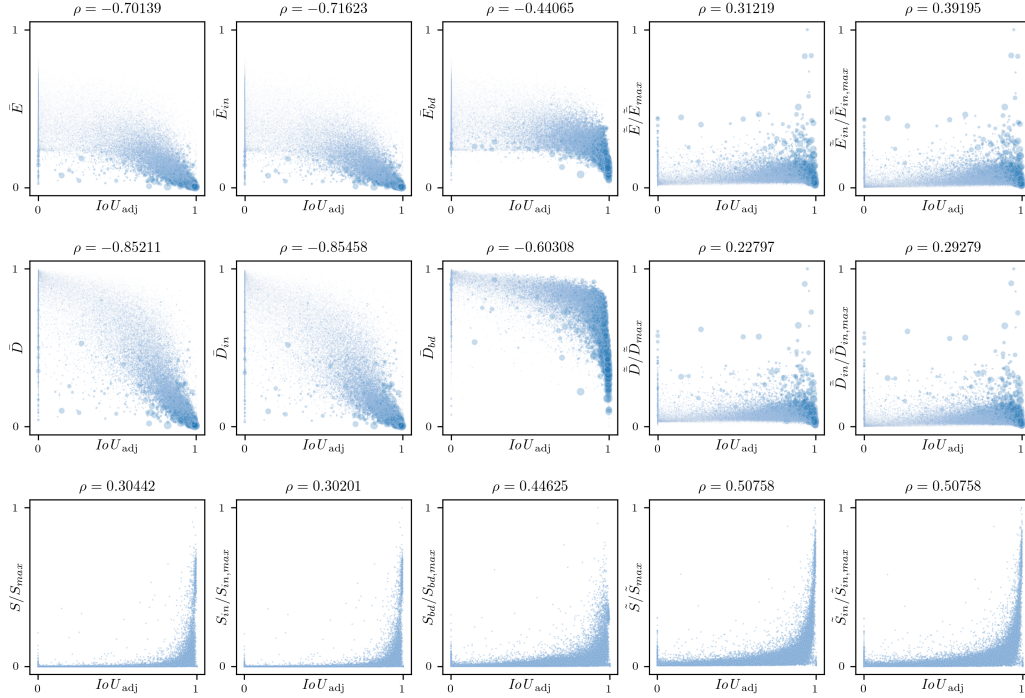


Figure 4. Correlations between IoU_{adj} and rescaled features for the DeepLabv3+Xception65 network. Dot sizes in the first two columns are proportional to S .

when only incorporating some of the metrics proposed by the LASSO trajectory. For both networks the classification accuracy corresponds to a logistic regression trained with unbalanced meta-classes $IoU_{adj} = 0$ and $IoU_{adj} > 0$, i.e., we did not adjust the class weights. On average (over the 10 training/validation splits) 6851 components with vanishing IoU_{adj} are detected for Xception65 while 4480 remain undetected, for MobilenetV2 this ratio is 14976/2695. These ratios can be adjusted by varying the probability thresholds for deciding between $IoU_{adj} = 0$ and $IoU_{adj} > 0$. For this reason we state results in terms of AUROC which is threshold independent. We compare our results with two different baselines in table 2. The naive baseline is given by random guessing (randomly assigning a probability to each segment k and then thresholding on it). The best meta classification accuracy is achieved for the threshold being either 0 or 1. For $I_0 = |\{k : IoU_{adj} = 0\}|$ and $I_1 = |\{k : IoU_{adj} > 0\}|$ the naive baseline accuracy is then given by $\frac{\max(I_0, I_1)}{I_0 + I_1}$. The corresponding AUROC value is 50%. Another baseline is to equip our approach only with a single metric. For this purpose we choose the entropy as it is commonly used for uncertainty quantification.

Ultimately, we want to predict IoU_{adj} values for all connected components and thus model an uncertainty measure. We now resign from regularization and use a linear regression model to predict the IoU_{adj} . Figure 2 depicts the quality of a single linear regression fit for each of

the two segmentation networks. For MobilenetV2 we obtain an R^2 value of 81.48% ($\pm 0.23\%$) and for Xception65 74.93% ($\pm 0.22\%$). Figure 5 illustrates the constructed uncertainty measure with two showcases. Averaged results over 10 runs including standard deviations σ and previous meta classification result are summarized in table 2. In all cases, the presented approach clearly outperforms the entropy. The linear regression models do not overfit the data and note-worthily we obtain prediction standard deviations of down to 0.130 and almost no standard deviation for the averages. The classification accuracy and AUROC results are slightly biased towards the validation results as they correspond to the particular λ value that maximizes the validation accuracy.

4. Numerical Experiments: Brain Tumor Segmentation

The method we propose only uses dispersion heat maps and softmax probabilities as inputs. Any additional heat map increases the performance as long as there is no overfitting. Thus, we expect our approach to generalize across different datasets even from different domains. To demonstrate this, we perform additional tests with the brain tumor segmentation dataset BraTS2017 [2, 17] and two different networks, i.e., a simple 2D network and a more complex 3D network. Compared to the segmentation of

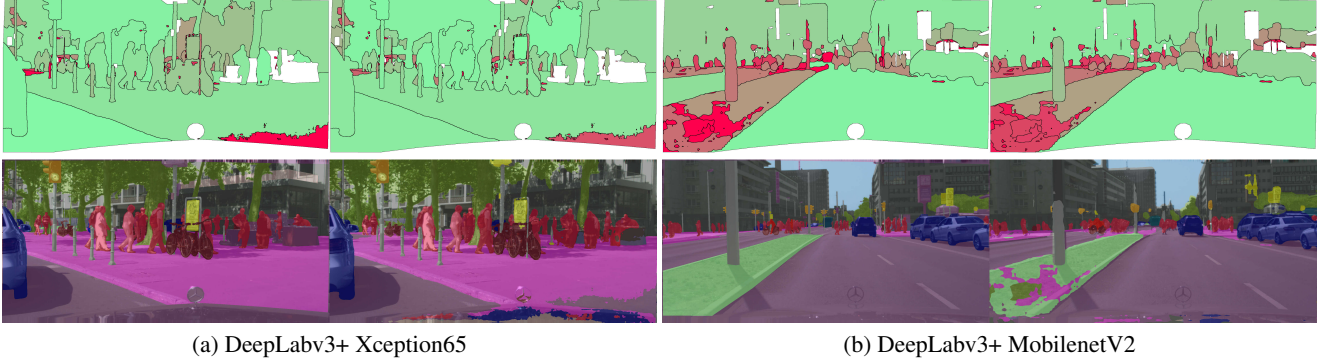


Figure 5. Prediction of the IoU_{adj} with linear regression. Each of the two sub-figures (a) and (b) consists of ground truth (bottom left), predicted segments (bottom right), true IoU_{adj} for the predicted segments (top left) and predicted IoU_{adj} for the predicted segments (top right). In the top row, green color corresponds to high IoU_{adj} values and red color to low ones, for the white regions there is no ground truth available. These regions are excluded from the statistical evaluation.

Cityscapes	Xception65		MobilenetV2	
	training	validation	training	validation
	Classification $IoU_{adj} = 0, > 0$			
ACC, penalized	81.88%(±0.13%)	81.91%(±0.13%)	78.87%(±0.13%)	78.93%(±0.17%)
ACC, unpenalized	81.91%(±0.12%)	81.92%(±0.12%)	78.84%(±0.14%)	78.93%(±0.18%)
ACC, entropy only	76.36%(±0.17%)	76.32%(±0.17%)	68.33%(±0.27%)	68.57%(±0.25%)
ACC, naive baseline	74.93%		58.19%	
AUROC, penalized	87.71%(±0.14%)	87.71%(±0.15%)	86.74%(±0.18%)	86.77%(±0.17%)
AUROC, unpenalized	87.72%(±0.14%)	87.72%(±0.15%)	86.74%(±0.18%)	86.76%(±0.18%)
AUROC, entropy only	77.81%(±0.16%)	77.94%(±0.15%)	76.63%(±0.24%)	76.74%(±0.24%)
	Regression IoU_{adj}			
σ , all metrics	0.181(±0.001)	0.182(±0.001)	0.130(±0.001)	0.130(±0.001)
σ , entropy only	0.258(±0.001)	0.259(±0.001)	0.215(±0.001)	0.215(±0.001)
R^2 , all metrics	75.06%(±0.22%)	74.97%(±0.22%)	81.50%(±0.23%)	81.48%(±0.23%)
R^2 , entropy only	49.37%(±0.32%)	49.02%(±0.32%)	49.32%(±0.31%)	49.12%(±0.32%)

Table 2. Summarized results for classification and regression for Cityscapes, averaged over 10 runs. The numbers in brackets denote standard deviations of the computed mean values.

street scenes, brain tumor segmentation involves way fewer classes. The background class is usually dominant. In BraTS2017, around 98% of all pixels are background, the remaining classes comprise necrotic/non-enhancing tumor, peritumoral edema and enhancing tumor. For benchmarks of predictive methods, these labels are combined into three nested classes: whole tumor (WT), tumor core (TC) and enhancing tumor (ET) (see figure 6). The most commonly used evaluation metric is the so-called *Dice-Coefficient* [25] that is defined as $Dice := 2TP / (2TP + FP + FN)$ where TP , FP and FN denote all true positive, false positive and false negative pixels, respectively, for a chosen class.

The BraTS data is available as magnetic resonance imaging (MRI) brain scans from three viewing angles and with four modalities of higher grade gliomas (HGG) and lower grade gliomas (LGG). For training and validation, we combine HGG and LGG images and randomly split the data 80/20. We train the networks from scratch with the different scan modalities stacked as network’s input channels. Once this is done, we perform tests analogously to the previous

section. The performance of the two networks being used on our validation split are reported in table 3, the results for classification and regression are summarized in table 4.

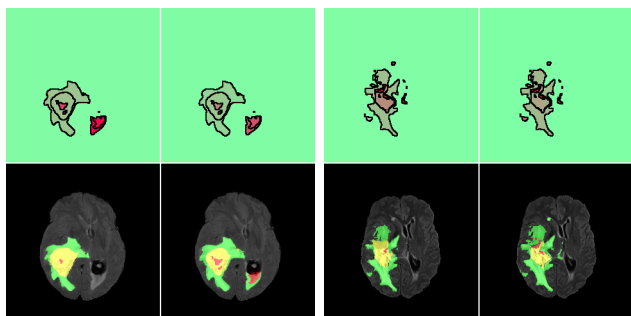
For the first test we use the network by Kermi et al. [14]. It is based on the U-Net [20] which is originally well-known for its performance on biomedical image segmentation. We train the network on randomly sampled 2D patches from axial (top view) slices of the brain scans. The results of our prediction rating methods are computed for 22,242 non-empty segments of which 2,603 have $IoU_{adj} = 0$. Indeed, we obtain higher accuracy values compared to Cityscapes, however the gain over the single metric baseline is not as big. This is primarily due to a strong correlation between E and IoU_{adj} (-0.87794). In this case, the gain over the naive baseline is marginal. This may be misleading to the disadvantage of our method as the high naive accuracy is caused by the strong sample imbalance of the meta-classes. The corresponding AUROC value of 91.93% shows that our method meta-classifies with significantly higher confidence when incorporating all metrics. Regarding the R^2 value of

Metric	Dice Coefficient				Intersection over Union	
	WT	TC	ET	$mDice$	$mIoU$ nested	$mIoU$ single
2D U-Net by Kermi et al.	88.09%	77.38%	78.89%	81.45%	68.99%	67.14%
3D Net by Myronenko et al.	88.83%	81.07%	79.63%	83.18%	71.40%	69.64%

Table 3. Evaluation scores on validation split. The nested classes whole tumor (WT), tumor core (TC) and enhancing tumor (ET) are evaluated with the Dice coefficient. For comparison purposes, the mean Dice score is reported as well as mean Intersection over Union for nested classes and single classes (background, non-enhancing tumor, peritumoral edema and enhancing tumor).

BraTS2017	2D U-Net by Kermi et al.		3D Net by Myronenko et al.	
	training	validation	training	validation
	Classification $IoU_{adj} = 0, > 0$			
ACC, penalized	89.30%(±0.18%)	89.39%(±0.17%)	88.40%(±0.27%)	88.42%(±0.27%)
ACC, unpenalized	89.29%(±0.19%)	89.40%(±0.18%)	88.38%(±0.27%)	88.40%(±0.28%)
ACC, entropy only	87.96%(±0.12%)	87.96%(±0.12%)	86.69%(±0.20%)	86.69%(±0.20%)
ACC, naive baseline	88.30%		86.35%	
AUROC, penalized	91.84%(±0.25%)	91.93%(±0.24%)	91.51%(±0.22%)	91.55%(±0.22%)
AUROC, unpenalized	91.83%(±0.25%)	91.93%(±0.24%)	91.49%(±0.22%)	91.53%(±0.22%)
AUROC, entropy only	86.68%(±0.25%)	86.73%(±0.25%)	86.59%(±0.28%)	86.74%(±0.28%)
	Regression IoU_{adj}			
σ , all metrics	0.148(±0.001)	0.149(±0.001)	0.171(±0.001)	0.171(±0.001)
σ , entropy only	0.178(±0.001)	0.178(±0.001)	0.198(±0.001)	0.197(±0.001)
R^2 , all metrics	84.22%(±0.21%)	84.15%(±0.21%)	79.53%(±0.28%)	79.64%(±0.28%)
R^2 , entropy only	77.18%(±0.18%)	77.30%(±0.17%)	72.63%(±0.27%)	72.91%(±0.27%)

Table 4. Summarized results for classification and regression for BraTS2017, averaged over 10 runs. The numbers in brackets denote standard deviations of the computed mean values.



(a) 2D U-Net by Kermi et al. (b) 3D Net by Myronenko et al.

Figure 6. Two demonstrations (left and right four panels, analogously to figure 5) of our method’s performance of predicting IoU_{adj} on BraTS2017. The whole tumor (WT) includes all colored segments (union of green, yellow & red), the tumor core (TC) the yellow joined with the red colored segments and the enhancing tumor (ET) only the yellow colored segments.

our regression model for predicting IoU_{adj} , we observe a gain from 77.30%(±0.17%) to 84.15%(±0.21%) when incorporating all metrics instead of only the entropy.

Next, we compare the U-Net’s performance to the state-of-the-art network by Myronenko et al. [18]. One main difference is that the latter network considers the MRI scans’ 3D contextual information by processing multiple contiguous 2D slices at once, i.e., we train the network on randomly sampled 3D patches. As a consequence, the model is more complex and the number of trainable parameters is noticeably increased (10.1M vs. 17.3M). We perform the evalu-

ation in the same 2D slice-wise manner as for the U-Net. The results are now computed for 24,397 non-empty segments of which 3331 have $IoU_{adj} = 0$. Again, we observe a strong correlation between E and IoU_{adj} of -0.84294 which results in a nearly identical gain in terms of percent points over the single metric baseline as for the U-Net. Also with respect to the R^2 value of our regression model, the gain is again around 7%, whereas the absolute value with 79.64%(±0.28%) for all metrics is not as high as for the U-Net. All results are summarized in table 4, the visualization in figure 6 further demonstrates the performance of our method.

5. Adjusted Intersection over Union

In section 2 we introduced the adjusted $IoU_{adj}(k)$ for an inferred segment $k \in \hat{\mathcal{K}}_x$ which slightly deviates from the ordinary $IoU(k)$. The reason for this is the following: In some cases it can happen that a connected component in the ground truth is split into two or more in the prediction. Each component would be assigned a moderate IoU value even though they are predicted very well (cf. also figure 7). For this reason we introduce the adjusted IoU_{adj} that does not depreciate the prediction of a segment if the remainder of the ground truth is well covered by other predicted segments belonging to the same class.

Clearly, we have $IoU_{adj}(k) = IoU(k) = 1$ if and only if the predicted segment k and the ground truth K' match for each pixel, $IoU_{adj} = IoU = |k \cap K'| = 0$ when ground truth and predicted segment do not overlap, i.e., $k \cap K' = \emptyset$,

	Xception65		MobilenetV2	
	training	validation	training	validation
	Regression IoU_{adj}			
σ , all metrics	0.181(± 0.001)	0.182(± 0.001)	0.130(± 0.001)	0.130(± 0.001)
σ , entropy only	0.258(± 0.001)	0.259(± 0.001)	0.215(± 0.001)	0.215(± 0.001)
R^2 , all metrics	75.06%($\pm 0.22\%$)	74.97%($\pm 0.22\%$)	81.50%($\pm 0.23\%$)	81.48%($\pm 0.23\%$)
R^2 , entropy only	49.37%($\pm 0.32\%$)	49.02%($\pm 0.32\%$)	49.32%($\pm 0.31\%$)	49.12%($\pm 0.32\%$)
	Regression IoU			
σ , all metrics	0.192(± 0.001)	0.192(± 0.001)	0.135(± 0.001)	0.135(± 0.001)
σ , entropy only	0.267(± 0.001)	0.268(± 0.001)	0.217(± 0.001)	0.217(± 0.001)
R^2 , all metrics	72.90%($\pm 0.21\%$)	72.77%($\pm 0.21\%$)	79.63%($\pm 0.27\%$)	79.58%($\pm 0.27\%$)
R^2 , entropy only	47.43%($\pm 0.28\%$)	47.07%($\pm 0.28\%$)	47.73%($\pm 0.37\%$)	47.50%($\pm 0.38\%$)

Table 5. Comparison of regression results for segment-wise fitting IoU_{adj} and IoU , averaged over 10 runs. The numbers in brackets denote standard deviations of the computed mean values.

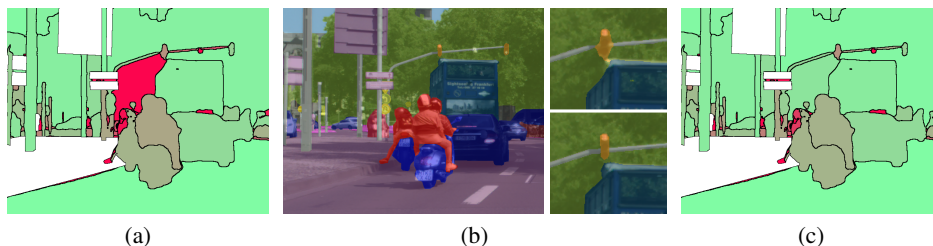


Figure 7. Illustration of the different behaviors of IoU and IoU_{adj} . We have (a): IoU per segment, (b) left: ground truth, right: detail views for the crucial area of the predicted segmentation (top) and the corresponding ground truth (bottom) and (c): IoU_{adj} per segment. Green stands for high IoU and IoU_{adj} values, red for low ones, respectively. The top right panel in (b) shows that the prediction for the class ‘nature’ is decoupled into two components by the traffic light’s prediction. The IoU rates this small part on the left from the traffic light very badly even though the prediction is absolutely fine. The adjusted IoU_{adj} circumvents this type of problems.

and it holds $IoU_{adj} \geq IoU$. Thus, the classification task is invariant under interchanging IoU and IoU_{adj} , however, the regression task is not.

Carrying out the regression tests from section 3 for the IoU_{adj} with the IoU as well, we observe that the regression fit for the IoU_{adj} achieves R^2 values that are roughly 2% higher than those for the IoU , cf. table 5. Usually, for performance measures in semantic segmentation, the IoU is computed for a chosen class over the whole image. This means that each pixel of the union of prediction and ground truth is only counted once in the denominator of the IoU . On the other hand, a ground truth pixel may contribute to IoU s of several segments. In this sense, in the context of semantic segmentation, the adjusted IoU_{adj} is closer in spirit to the regular image-wise IoU .

It seems natural to consider an intersection over segment size $IoS(k) = |k \cap K'|/S$ as well. However, $IoS(k) = 1$ for a segment k does not imply that a segment perfectly matches the corresponding ground truth. Consequently, one should refrain from considering this measure, at least as an exclusively used performance measure.

6. Conclusion and Outlook

We have shown statistically that per-segment metrics derived from entropy, probability difference, segment size

and the predicted class clearly contain information about the reliability of the segments and constructed an approach for detecting unreliable segments in the network’s prediction. In our tests with publicly available networks and datasets, Cityscapes and BraTS2017, the computed logistic LASSO fits for meta classification task $IoU_{adj} = 0$ vs. $IoU_{adj} > 0$ achieve AUROC values of up to 91.55%. When predicting the IoU_{adj} with a linear regression fit we obtain a prediction standard deviation of down to 0.130, as well as R^2 values of up to 84.15%. These results could be further improved when incorporating model uncertainty in heat map generation. We believe that using MC dropout will further improve these results, just like the development of ever more accurate networks. We plan to use our method for detecting labeling errors, for label acquisition in active learning and we plan to investigate further metrics that may leverage detection accuracy. Apart from that, detection mechanisms built on the softmax input and even earlier layers could be thought of. The source code of our method is publicly available at <https://github.com/mrothmann/MetaSeg>.

Acknowledgements. This work is funded in part by Volkswagen Group Innovation.

References

- [1] M. Abadi, A. Agarwal, P. Barham, et al. TensorFlow: Large-scale machine learning on heterogeneous systems, 2015. Software available from tensorflow.org. **3**
- [2] S. Bakas, H. Akbari, A. Sotiras, M. Bilello, M. Rozycki, J. S. Kirby, J. B. Freymann, K. Farahani, and C. Davatzikos. Advancing the cancer genome atlas glioma mri collections with expert segmentation labels and radiomic features. *Scientific Data*, 4, Sep 2017. Data Descriptor. **2, 5**
- [3] L.-C. Chen, Y. Zhu, G. Papandreou, F. Schroff, and H. Adam. Encoder-decoder with atrous separable convolution for semantic image segmentation. *CoRR*, abs/1802.02611, 2018. **3**
- [4] F. Chollet. Xception: Deep learning with depthwise separable convolutions. *2017 IEEE Conference on Computer Vision and Pattern Recognition (CVPR)*, pages 1800–1807, 2017. **3**
- [5] M. Cordts, M. Omran, S. Ramos, T. Rehfeld, M. Enzweiler, R. Benenson, U. Franke, S. Roth, and B. Schiele. The cityscapes dataset for semantic urban scene understanding. In *Proc. of the IEEE Conference on Computer Vision and Pattern Recognition (CVPR)*, 2016. **2, 3**
- [6] F. Cowell. *Measuring Inequality*. Oxford Univ. Press, 2011. **2**
- [7] J. Davis and M. Goadrich. The relationship between precision-recall and ROC curves. In *Machine Learning, Proceedings of the Twenty-Third International Conference (ICML 2006), Pittsburgh, Pennsylvania, USA, June 25-29, 2006*, pages 233–240, 2006. **2**
- [8] Y. Gal and Z. Ghahramani. Dropout as a bayesian approximation: Representing model uncertainty in deep learning. In *Proceedings of the 33rd International Conference on International Conference on Machine Learning - Volume 48, ICML'16*, pages 1050–1059. JMLR.org, 2016. **1**
- [9] D. Hendrycks and K. Gimpel. A baseline for detecting misclassified and out-of-distribution examples in neural networks. *CoRR*, abs/1610.02136, 2016. **1**
- [10] P.-Y. Huang, W.-T. Hsu, C.-Y. Chiu, T.-F. Wu, and M. Sun. Efficient uncertainty estimation for semantic segmentation in videos. In *European Conference on Computer Vision (ECCV)*, 2018. **1**
- [11] P. Jaccard. The distribution of the flora in the alpine zone. *New Phytologist*, 11(2):37–50, Feb. 1912. **2**
- [12] M. Kampffmeyer, A.-B. Salberg, and R. Jenssen. Semantic segmentation of small objects and modeling of uncertainty in urban remote sensing images using deep convolutional neural networks. *2016 IEEE Conference on Computer Vision and Pattern Recognition Workshops (CVPRW)*, pages 680–688, 2016. **1**
- [13] A. Kendall, V. Badrinarayanan, and R. Cipolla. Bayesian segnet: Model uncertainty in deep convolutional encoder-decoder architectures for scene understanding. *CoRR*, abs/1511.02680, 2015. **1**
- [14] A. Kermi, I. Mahmoudi, and M. T. Khadir. Deep convolutional neural networks using u-net for automatic brain tumor segmentation in multimodal mri volumes. In *International MICCAI Brainlesion Workshop*, pages 37–48. Springer, 2018. **6**
- [15] S. Liang, Y. Li, and R. Srikant. Principled detection of out-of-distribution examples in neural networks. *CoRR*, abs/1706.02690, 2017. **1**
- [16] W. Lin and A. Hauptmann. Meta-classification: Combining multimodal classifiers. *Mining Multimedia and Complex Data. PAKDD 2002. Lecture Notes in Computer Science*, 2797, 2003. **1**
- [17] B. H. Menze, A. Jakab, S. Bauer, J. Kalpathy-Cramer, K. Farahani, J. Kirby, Y. Burren, N. Porz, J. Slotboom, R. Wiest, et al. The multimodal brain tumor image segmentation benchmark (brats). *IEEE Transactions on Medical Imaging*, 34(10):1993–2024, Oct 2015. **2, 5**
- [18] A. Myronenko. 3D MRI brain tumor segmentation using autoencoder regularization. In A. Crimi, S. Bakas, H. Kuijff, F. Keyvan, M. Reyes, and T. van Walsum, editors, *Brainlesion: Glioma, Multiple Sclerosis, Stroke and Traumatic Brain Injuries*, pages 311–320, Cham, 2019. Springer International Publishing. **7**
- [19] P. Oberdiek, M. Rottmann, and H. Gottschalk. Classification uncertainty of deep neural networks based on gradient information. In *Artificial Neural networks and Pattern Recognition (ANNPR)*, 2018. **1**
- [20] O. Ronneberger, P. Fischer, and T. Brox. U-net: Convolutional networks for biomedical image segmentation. In N. Navab, J. Hornegger, W. M. Wells, and A. F. Frangi, editors, *Medical Image Computing and Computer-Assisted Intervention – MICCAI 2015*, pages 234–241, Cham, 2015. Springer International Publishing. **6**
- [21] M. Sandler, A. G. Howard, M. Zhu, A. Zhmoginov, and L.-C. Chen. Inverted residuals and linear bottlenecks: Mobile networks for classification, detection and segmentation. *CoRR*, abs/1801.04381, 2018. **3**
- [22] C. E. Shannon. A mathematical theory of communication. *The Bell System Technical Journal*, 27:379–423, 623–656, 1948. **2**
- [23] R. Tibshirani. Regression shrinkage and selection via the lasso. *Journal of the Royal Statistical Society: Series B*, 58:267–288, 1996. **4**
- [24] K. Wickstrøm, M. Kampffmeyer, and R. Jenssen. Uncertainty and interpretability in convolutional neural networks for semantic segmentation of colorectal polyps. *CoRR*, abs/1807.10584, 2018. **1**
- [25] K. H. Zou, S. K. Warfield, A. Bharatha, C. M. C. Tempany, M. R. Kaus, S. J. Haker, W. M. r. Wells, F. A. Jolesz, and R. Kikinis. Statistical validation of image segmentation quality based on a spatial overlap index. *Academic radiology*, 11(2):178–189, Feb 2004. **6**